EXPERIMENTAL

The SAXS instrument was constructed at ANL and used on the Basic Energy Sciences Synchrotron Radiation Center CAT undulator beamline ID-12 at the Advanced Photon Source (http://www.bessrc.aps.anl/). The SAXS instrument has been designed to minimize parasitic scattering which would interfere with scattering from dilute samples such as soots in flames. An important key to this feature of the instrument is that the beam is defined 20 m from the sample which reduces the problem of scattering from the defining slits. A schematic of the instrument is shown in Scheme 1.

Monochromatic X-rays (8.5 - 23.0 keV) are scattered off the sample and collected on a 9-element mosaic CCD detector (15 x 15 cm) with maximum of 3000 x 3000 pixel resolution with 10 sec exposure times (9). The scattered intensity has been corrected for absorption, the air scattering, and instrument background. The differential scattering cross section has been expressed as a function of the scattering vector Q, which is defined as $Q = (4\pi/\lambda) \sin \theta$, where λ is the wavelength of the X-rays and θ is the scattering half angle. The value of Q is proportional to the inverse of the length scale ($Å^{-1}$). The instrument was operated with two different sample-to-detector distances, 68.5 cm to obtain data at $0.04 < Q < 0.7$ $Å^{-1}$ and 3740 cm to measure at $0.006 < Q < 0.1$ $Å^{-1}$.

The Argonne Premium Coal Samples (10) used in this study were sized to the range of 45-75 μm. The burner used for these studies was a 1" x 1" axial symmetric flat flame burner produced by Research Technologies. The coal and liquids were fed through a tube centered in the burner and, a 0.25" nitrogen and helium co-flow around the perimeter was used to stabilize the methane/hydrogen flame. The individual coal particles were fed to the flame using a technique which that has previously been described (5). Liquid samples were introduced into the flame via a 0.25 μm fused silica tube which protruded 2 mm above the surface of the burner. Samples such as toluene and heptane were flowed into the flame at 0.1 ml using an automated syringe.

The burner was mounted on a x-y translational stage such that the flame could be moved through the X-ray beam both vertically and horizontally.

Small Angle X-ray Scattering

A typical plot of the scattering data for soot formation as a function of distance from the top of the burner of the Illinois No. 6 bituminous coal (APCS 3) is shown in Figure 1. These curves can be analyzed to determine size of features, topology, and changes in total scattering. Power law slope from the data, such as is shown in Figure 1, are used to describe the topology of the system. Finally, the invariant Q_0 is calculated and is proportional to the fluctuation of the electron density in the system. Changes in the invariant are useful in monitoring topological changes in the sample, $Q_0 = \int_0^\infty I(Q)\, Q^2\, dQ$. For example, the invariant goes to zero for a homogeneous system that does not have any concentration fluctuation.

RESULTS AND DISCUSSION

The scattering data were obtained as the burner was moved in 1 mm steps, such that the X-ray beam passed through the flame vertically from the bottom (0 mm) to 40 mm above the bottom. In addition, vertical sets of data were collected as the beam was positioned on center, where the coal particles emerged, and 1 ml increments from the center. The Illinois No. 6 (APCS 3) data from a vertical set at the center of the burner is shown in Figure 1. An initial Guinier analysis of this data suggests that the particle sizes are polydispersed over the section of the flame where soot is observed. Also, there are no systematic changes in the invariant. However, as can be seen in Figure 2, the power law slope is increasing. This suggests that there is a roughening in the soot particle surface. Note the large amount of scatter in the data. This may mean that a wide range of soot particles are observed, or else that there is merely a lot of scatter in the data. With combustion of the coal particles, the scattering decreased rapidly as the X-ray beam is moved away from the center (not shown) and becomes difficult to measure at 3 mm from the center.

Hydrocarbons, such as toluene, gave much better data in this system than coal particles. The flame conditions and the data acquisition parameters are the same in both cases, but apparently a much more stable soot cloud results from the direct infusion of the aromatic hydrocarbon. The power law slope data for the toluene ($Q = 0.016$ to 0.04) is shown in Figure 3. For the first 5-10 mm of the lower part of the flame, the value of $d_o = 2.0$, strongly suggests that larger polycyclic aromatic

expected, the scattering for the combustion of heptane (not shown) was much less than that for toluene.

CONCLUSIONS

Some of the initial results look promising, but we need a low flame temperature in order to observe the intermediate sized particles. This approach may reduce the polydispersity.

ACKNOWLEDGMENTS

This work was performed under the auspices of the Office of Basic Energy Sciences, Division of Chemical Sciences, U.S. Department of Energy, and use of the Advanced Photon Source was supported by BES-DOE, all under contract number W-31-109-ENG-38. The support of the BESSRC staff is appreciated, especially J. Linton, M. Beno, G. Jennings, and M. Engbretson.

REFERENCES

1. DOE-BES Facilities Initiative entitled "Development of a Facility at APS for Time-Resolved/Anomalous Small Angle X-ray Scattering: Applications in Condensed Matter Research," R. E. Winans, P. Thiyagarajan, R. K. Crawford, K. A. Carrado, and D. M. Tiede.
2. McLean, W. M.; Hardesty, D. R.; and Poll, J. H. Proc., 18th Symp. (Int'l.) Combust., 1213 (1980).
3. England, W. A. *Combust. Sci. and Tech.* **1986**, *46*, 83-93.
4. Köylü, Ü. Ö. *Combustion and Flame* **1996**, *109*, 488-500.
5. Ma, J.; Fletcher, T. H.; Webb, B. W. *Energy Fuels* **1995**, *9*, 802-808.
6. Ragucci, R.; De Joannon, M.; Cavaliere, A. Proc., 26th Symp. (Int'l.) Combust., Vol. 2, 2525-2531 (1996).
7. T. Freltoft, J. K. Kjems, S. K. Sinha, Phys. Rev. B. 33, 269-275 (1986).
8. Cody, G. D.; Thiyagarajan, P.; Botto, R. E.; Hunt, J. E.; Winans, R. E. *Energy Fuels* **1994**, *8*, 1370-1378 (1994).
9. Westbrook, E. M.; Naday, I. *Methods Enzymol.* **1997**, *276*, 244-268.
10. Vorres, K. S. *Energy Fuels* **1990**, *4*, 420-426.

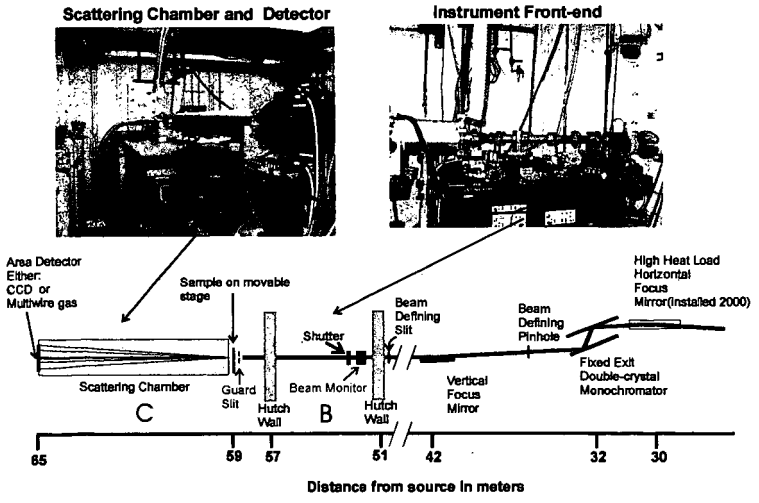

Scheme 1. TR/ASAXS Instrument on the APS BESSRC ID-12-B&C Undulator Beamline

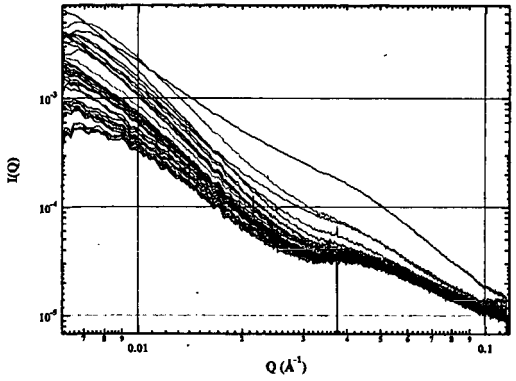

Figure 1. Scattering from Illinois coal (APCS 3) taken at 1 mm intervals from 0 to 40 mm above the top of the burner centered.

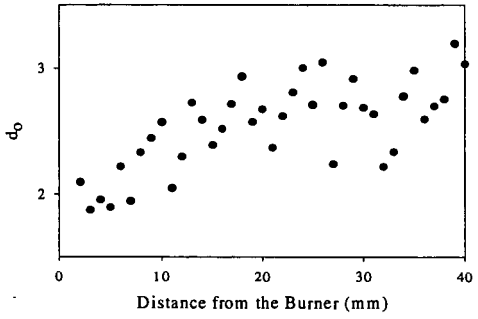

Figure 2. Power law slope from scattering of Illinois coal (APCS 3) soot taken along the centerline at 1 mm intervals from 0 to 40 mm above the top of the burner.

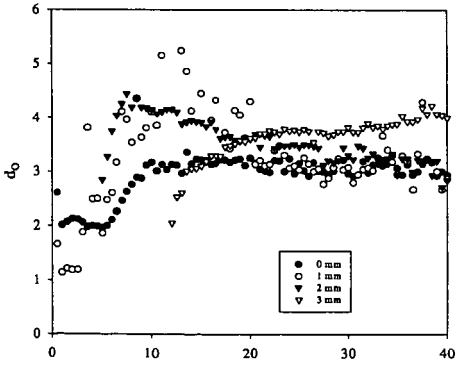

Figure 3. Power law slope from scattering of toluene soot taken at 1 mm intervals from 0 to 40 mm above the top of the burner at 1 mm intervals from the center.

For comparison, the nickel-impregnated coals were also prepared. About 1 g of raw coal was immersed in an aqueous solution containing about 6 or 12 wt % of nickel chloride and the water in this mixture was evaporated at 323 K under vacuum using rotary evaporator. The pH of the solution was controlled by using HCl or NH_3. The impregnated samples are identified using an additional code indicating impregnation (Im) and the pH at the time of impregnation, e.g., 10.51Ni (Im, pH3) for the specimen impregnated with 10.51 wt% nickel from solution of pH 3.

2.2 C1 Gas Analysis. The pyrolysis experiment was carried out in a fixed-bed-type pyrolyzer under helium flow at a heating rate of 5 K/min from 373 to 1173 K, and the evolved C1 gases were analyzed every 6 min by a gas chromatograph attached to the pyrolyzer.

2.3 Infrared Spectroscopy. Coal samples were diluted to 3 wt% by mixing of potassium bromide. Infrared spectra were obtained by diffuse reflectance method using a Perkin-Elmer 1600 Series FT-IR spectrometer.

2.4 XAFS. The details of procedure were described previously.[8-9] Briefly, data were collected at beam lines BL–7C, –10B, and –12C at the Photon Factory. Data were recorded in the transmission mode in the region of the Ni K edge (8331.7 eV) at room temperature. The transmission spectra were collected using ion chambers that were filled with nitrogen gas. EXAFS oscillation was extracted from the EXAFS raw data by using a cubic spline method and normalized with the edge height. The k^3-weighted EXAFS spectra were Fourier transformed to R space. The inversely Fourier filtering data were analyzed by a curve-fitting technique on the basis of the single-scattering plane-wave theory. Experimentally determined phase shifts and backscattering amplitudes for Ni-Ni and Ni-O were obtained from EXAFS data for Ni foil (Ni-Ni; coordination number (N) = 12, distance (R) =2.488 Å) and NiO (Ni-O; N = 6, R = 2.098 Å), respectively.

3. RESULTS AND DISCUSSION

3.1 C1 Gas Evolution. Typical C1 gas evolution profiles are given in Fig. 1. Obviously, the gas evolution was affected by the presence of nickel. The main features in the nickel-exchanged coals can be summarized as follows. The evolved CO gas shown in Figure 1(b) – (d) consisted of two peaks; one at 670 – 770 K and the other at around 920 K. When the nickel content was increased, the former peak shifted to lower temperature by 100 K but was almost the same in height. On the other hand, the latter peak height increased with the nickel contents, notably in the region below 3 wt%. For CO_2 evolution, it was seen that main peak shifted to lower temperature by 20 - 30 K compared to AW coal. The CO_2 evolution in the higher temperature region, above 800 K, was negligibly small for nickel content below 3 wt%, whereas the CO_2 in this region increased with the amount of nickel above 3 wt%. The CH_4 evolved profile had a small decrease in the middle temperature region between 720 and 870 K, possibly due to the nickel catalyzing secondary decomposition.

For nickel-impregnated coals, C1 gas evolution profiles are also shown in Figure 1. When the pH of the solution was low (Fig. 1(e)), C1 gas profile was similar to that of AW coal. On the contrary, C1 gas profile of sample prepared in the high pH of the solution (Fig. 1(f)) was similar to that prepared by ion exchange method.

The total gas evolution versus metal loading is presented in Fig. 2. The filled marks in this figure indicate the gas evolution from the impregnated coal. The effects of metal observed here consist of those metal-catalyzed decomposition of functional groups and the secondary conversion of oxygen containing volatiles into CO and CO_2 catalyzed by metal elements. From this figure, CO yields remarkably increased from 8% to 15% with increasing nickel loadings from 0 to about 3 %, whereas CO_2 yields were almost constant at about 7% in the same region of nickel contents. Above 3wt% of nickel loadings, CO and CO_2 yields gradually increased. It seems that the exchanged nickel below and above about 3 wt% differ somewhat in the way it affects the decomposition, whereas the impregnated nickel behaved quite differently and yielded less gases than the exchanged nickel.

These differences can be ascribed to a different state of nickel species. In the case of ion exchange, nickel ions are associated with carboxyl groups. On the other hand, most of nickel species loaded by impregnation method would form a cluster of the metal salt and, upon decomposition, distribute over the entire coal surface and not limited specifically to functional group sites. Therefore, it is likely that the exchanged nickel ions have a stronger influence than the impregnated species on the decomposition of functional groups in coal.

3.2 *States of nickel species after ion exchange.* For the nickel-exchanged coals, it is very interesting to change the pyrolysis behavior below and above 3 wt% of nickel loadings. In order to examine the chemical state of the exchanged nickel ions in brown coal, FT-IR measurement was carried out. Figure 3 shows the IR spectra of brown coals with various

exchanged nickel contents. The differences of IR spectra between AW and the nickel-exchanged coal are also shown in this figure. From this figure, it was found that the absorption band of carboxyl groups, which appeared at 1720 cm^{-1}, decreased with increasing nickel contents. On the contrary, the bands of OCO asymmetric stretching (ν_a) at 1550 cm^{-1} and OCO symmetric stretching (ν_s) at 1480 – 1410 cm^{-1} of carboxylate groups increased. It should be noted that the peak position of ν_s band depended on the amount of the exchanged nickel. The peak at 1480 cm^{-1} in low nickel loaded sample was dominant, but in high nickel loaded sample the peak at 1410 cm^{-1} was dominant. This suggests that the chemical state of nickel species differs by the nickel content. According to reference, it was found that this difference of peak position corresponded with the difference of the structure of carboxylate groups; the nickel ions in low loaded sample were associated with carboxyl groups in the form of bidentate-type, while those in high loaded sample were in the form of bridge-type.

3.3 EXAFS. To examine how such differences in the chemical form of nickel species influence on the behavior of nickel species during pyrolysis, EXAFS experiments was carried out. Figure 4 shows the Fourier transforms for EXAFS spectra of the 0.77Ni and 6.4Ni samples pyrolyzed from 373 to 853 K. From Fourier transformed EXAFS spectra of both nickel exchanged coals at 373 K, only Ni-O bond appeared between 1 and 2 Å was observed, indicating that the nickel species were highly dispersed on the brown coal surface independent of nickel loadings. The intensity of Ni-O bond decreased with increasing heat treatment temperature, while new peak around 2.5 Å, which was attributed to Ni-Ni bond, was appeared and its intensity increased. That is, the divalent nickel ions were reduced to the metallic state during pyrolysis. More interestingly, the transition temperature from divalent cations to metal particles depended on the nickel contents. Figure 5 shows the dependence of Ni-Ni coordination numbers on the pyrolysis temperatures. Nickel species in the low loaded sample aggregated to metal particles at 750 K. On the other hand, nickel species aggregated at 650 K in the high loaded sample. The transition temperature for the low loaded sample was 100 K higher than that of the high loaded sample. These transition temperatures corresponded with temperatures of the former CO peak described previously, which appeared at 770 K in the low loaded sample and at 670 K in the high loaded sample. The peak shift at about 100 K suggests that the states of nickel species in coal and their effects are different according to the nickel amounts. We suppose that the metallic nickel particle formation is related to the decomposition of carboxyl groups / CO evolution.

4. CONCLUSIONS

The following conclusions are obtained in this study.

(1) At the initial stage of pyrolysis, the exchanged nickel influenced on the decomposition of functional groups.

(2) The chemical structure of nickel carboxylate groups differs by the nickel content; the nickel ions in low loaded sample were associated with carboxyl groups in the form of bidentate-type, while those in high loaded sample were in the form of bridge-type.

(3) By using XAFS technique, the aggregation temperature of nickel species, which was 750 K at low loaded sample, was observed to have shifted to lower temperature by 100K at high loaded sample.

References

(1) Otake, Y., and Walker Jr., P. L., *Fuel*, **72** (1993) 139.
(2) Tyler, R. J., and Schafer, H. N. S., *Fuel*, **59** (1980) 487.
(3) Franklin, H. D., Peters, W. A., and Howard, J. B., *Fuel*, **61** (1982) 155.
(4) Schafer, H. N. S., *Fuel*, **58** (1979) 667.
(5) Schafer, H. N. S., *Fuel*, **58** (1979) 673.
(6) Murakami, K., Shirato, H., Ozaki, J., and Nishiyama, Y., *Fuel Process. Tech.*, **46** (1996) 183.
(7) Murakami, K., Ozaki, J., and Nishiyama, Y., *Fuel Process. Tech.*, **43**, (1995) 95.
(8) Shirai, M., Murakami, K., and Nishiyama, Y., *Energy Fuels*, **11** (1997) 1012.
(9) Shirai, M., Arai, M., and Murakami, K., *Energy Fuels*, **13** (1999), 465.

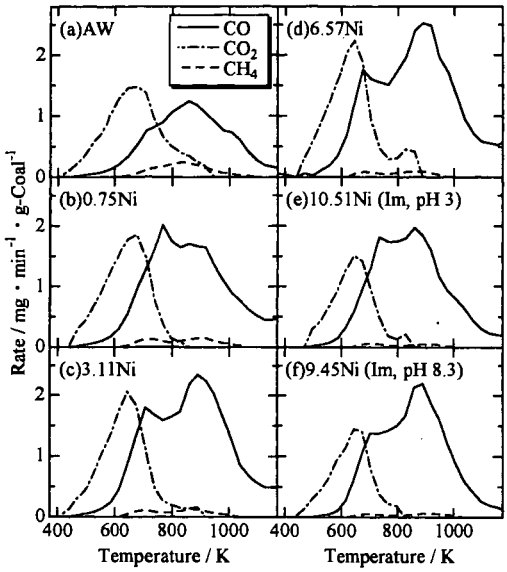

Figure 1. C1 gas evolution profiles of AW, nickel-exchanged coals, and nickel-impregnated coals.

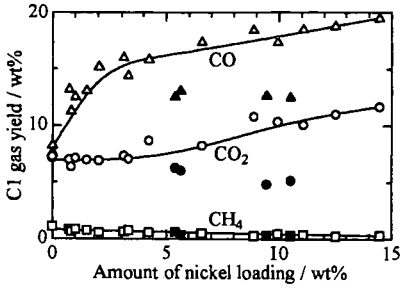

Figure 2. Change of C1 gas yields with the amount of nickel loading. Filled marks indicates impregnated samples.

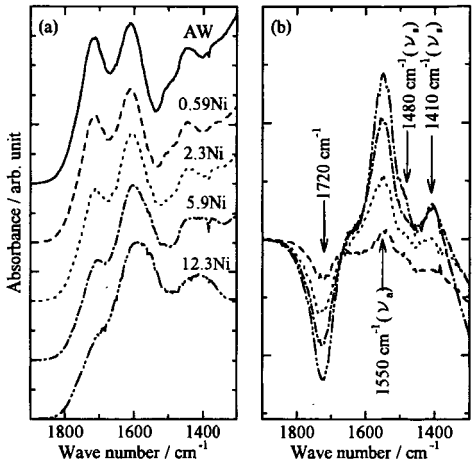

Figure 3. (a) IR spectra and (b) difference spectra of the nickel exchanged coals.

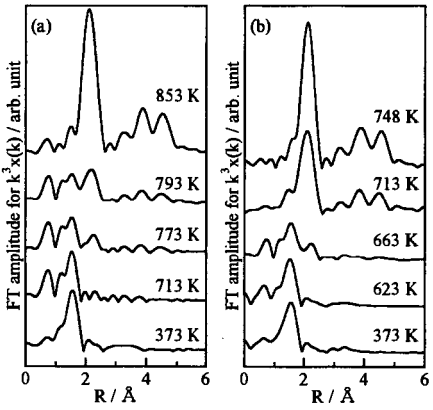

Figure 4. Fourier transforms for EXAFS oscillations of (a) 0.77Ni and (b) 6.4Ni nickel-loaded brown coals treated at several temperatures. These distributions were obtained by the Fourier transforms of the k^3-weighted EXAFS data.

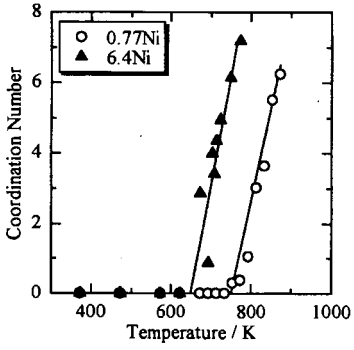

Figure 5. Coordination numbers of Ni-Ni bonds as a function of treatment temperature.